Symmetrical and unsymmetrical quadruply Aza bridged closely interspaced cofacial Bis(5,10,15,20-tetraphenylporphyrin)s. 3. Interplanar distances, 1H NMR chemical shifts, and the ca...

ARTICLE *in* JOURNAL OF THE AMERICAN CHEMICAL SOCIETY · JUNE 1992

Impact Factor: 12.11 · DOI: 10.1021/ja00038a066

4 AUTHORS, INCLUDING:

Rafik Karaman
Al-Quds University
204 PUBLICATIONS **2,197** CITATIONS
SEE PROFILE

Orn Almarsson
Moderna
43 PUBLICATIONS **3,161** CITATIONS
SEE PROFILE

Symmetrical and Unsymmetrical Quadruply Aza Bridged Closely Interspaced Cofacial Bis(5,10,15,20-tetraphenylporphyrin)s. 3. Interplanar Distances, ^{1}H NMR Chemical Shifts, and the Catalysis of the Electrochemical Reduction of Oxygen

Rafik Karaman, Seungwon Jeon, Örn Almarsson, and Thomas C. Bruice*

Contribution from the Department of Chemistry, University of California at Santa Barbara, Santa Barbara, California 93106. *Received November 4, 1991*

Abstract: The gas-phase geometries of the aza bridged cofacial porphyrin dimers **1-7** were calculated by the CHARM$_m$ molecular dynamics method. It was found that the global minimum conformations of porphyrins **1-5** have a D_4 symmetry and those of dimers **6** and **7** have a C_2 symmetry. Electrochemical (rotating ring-disk electrode) reduction of O_2 via cobalt complexes of **1-4** and **6** establish both pathways of 4e$^-$ reduction (to form water) and 2e$^-$ reduction (to furnish hydrogen peroxide). The geometry and the center-to-center distance (Ct-Ct) between the two porphyrin cores in the dimers are crucial factors for determining the electroreduction pathway. Biscobalt dimers with Ct-Ct distances of less than 5 Å catalyze the reduction of dioxygen mainly through the 4e$^-$ pathway, whereas those with Ct-Ct distances > 5.35 Å do via the 2e$^-$ path. In contrast to the observations of Collman and Chang, we find that the peak potentials for the 4e$^-$ reduction of O_2 via biscobalt porphyrin dimers **1-4** and **6** are comparable to that of the 2e$^-$ reduction by the monocobalt porphyrin **8**. Therefore, the precise geometry of the biscobalt tetraphenylporphyrin dimer is the crucial factor that determines 2e$^-$ vs 4e$^-$ reduction of O_2 while the reduction potential is independent of the path. The biscobalt cofacial porphyrins **1** and **2** represent the first rigid metalloporphyrin dimer system to catalyze effectively the 4e$^-$ reduction of O_2 to water. Further, a linear correlation has been found between the solution ^{1}H NMR chemical shifts of the pyrrolic N-H resonances (δ' NH) and the number of electrons transferred (n) in the reduction of dioxygen catalyzed by biscobalt dimeric porphyrins.

Introduction

A present goal in the mimicking of enzymatic catalysis is to position in purposeful proximity two porphyrin cores such that they may jointly enter into reactions.[1] The groups of Collman and Chang have prepared covalently linked porphyrin dimer systems in which the two metals in the centers of the porphyrin rings interact in a concerted fashion in the binding of O_2 and N_2.[1] They were able to show that flexible dimers such as an anthracene pillar dicobalt porphyrin (having slipping flexibility) and dicobalt porphyrins linked by two amide chains between diametrical β-positions (Chart I) are capable of reducing dioxygen to water via the four-electron-reduction pathway without the intermediacy of hydrogen peroxide. On the other hand, they found that rigid systems with inappropriate center-to-center distances (Chart II) precluded any concerted coordination of the dioxygen molecule to the cobalt located in the centers of the porphyrin cores.[2]

Herein we report the first example of rigid water-soluble bisporphyrin structures (quadruply aza bridged closely interspaced cofacial biscobalt 5,10,15,20-tetraphenylporphyrins) which act as effective catalysts for the four-electron reduction of dioxygen to water.

Results and Discussion

Theoretical Calculations. The center-to-center distance is believed to be a determining factor for the efficiency of cofacial porphyrin dimers as electroreduction catalysts capable of catalyzing the 4e$^-$ reduction of dioxygen to water.[2] Thus, knowledge

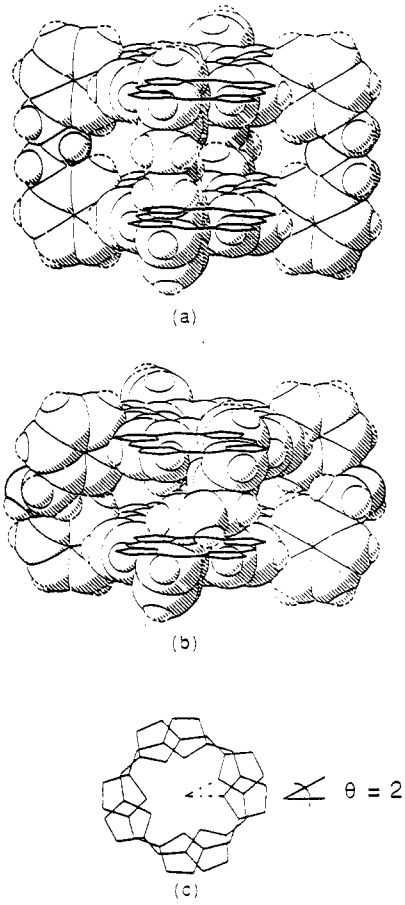

Figure 1. (a) Shaded CPK model of the totally extended form of the porphyrin dimer. (b) Shaded CPK model of the totally screwed down form of the porphyrin dimer. (c) Distal view line drawing of the porphyrin rings of the totally screwed down form illustrating the angle $\Phi_{N1Ct2N2}$.

(1) (a) Collman, J. P.; Marrocco, M.; Denisevich, P.; Koval, C.; Anson, F. C. *J. Electroanal. Chem.* **1979**, *101*, 117. (b) Collman, J. P.; Denisevich, P.; Konai, Y.; Marrocco, M.; Koval, C.; Anson, F. C. *J. Am. Chem. Soc.* **1980**, *102*, 6027. (c) Geiger, T.; Anson, F. C. *J. Am. Chem. Soc.* **1981**, *103*, 7489. (d) Liu, H. Y.; Abdalmuhdi, I.; Chang, C. K.; Anson, F. C. *J. Phys. Chem.* **1985**, *89*, 665. (e) Liu, H. Y.; Weaver, M. J.; Wang, C.-B.; Chang, C. K. *J. Electroanal. Chem.* **1983**, *145*, 439. (f) Sawaguchi, T.; Matsue, T.; Itaya, K.; Uchida, I. *Electrochim. Acta* **1991**, *36*, 703. (g) Collman, J. P.; Hendricks, N. H.; Leidner, C. R.; Ngameni, E.; L'Her, M. *Inorg. Chem.* **1988**, *27*, 387. (h) Durand, R. R., Jr.; Bencosme, C. S.; Collman, J. P.; Anson, F. C. *Ibid.* **1983**, *105*, 2710. (i) Chang, C. K.; Liu, H. Y.; Abdalmuhdi, I. *J. Am. Chem. Soc.* **1984**, *106*, 2725. (j) Chang, C. K. *Adv. Chem. Ser.* **1979**, *173*, 162.

(2) Collman, J. P.; Anson, F. C.; Bencosme, S.; Chong, A.; Collins, T.; Denisevich, P.; Evitt, E.; Geiger, T.; Ibers, J. A.; Jameson, G.; Konai, Y.; Koval, C.; Meier, K.; Okaley, P.; Pettman, R.; Schmittou, E.; Sessler, J. In *Organic Synthesis Today and Tomorrow*; Trost, B. M.; Hutchinson, C. R., Eds.; Pergamon Press: Oxford, 1981; pp 29-45.

0002-7863/92/1514-4899$03.00/0

Chart I

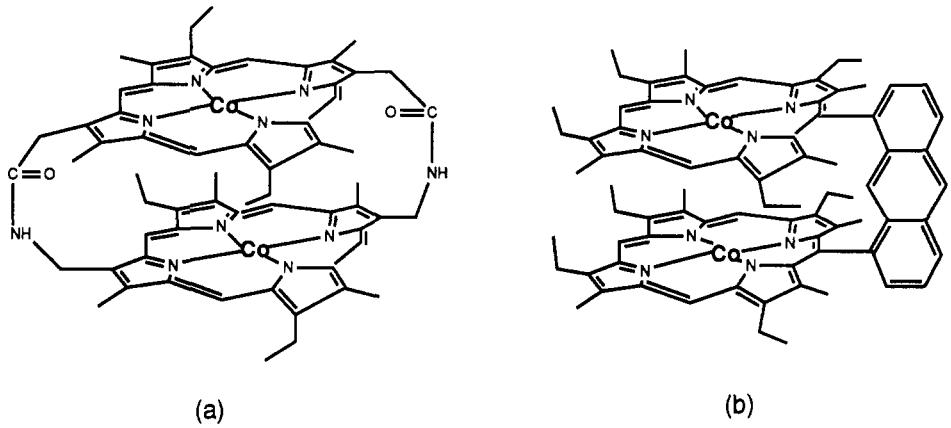

(a) (b)

[a] (a) Doubly bridged dicobalt porphyrin linked via amide chains between diametrical β-positions. (b) An anthracene pillar dicobalt porphyrin.

of the geometrical structure of the dimeric porphyrin is imperative in predicting the efficacy of the catalyst. We have used the molecular mechanics empirical forcefield CHARM$_m$[3] to calculate geometries for the dimeric porphyrins **1**–**7**. The calculations were

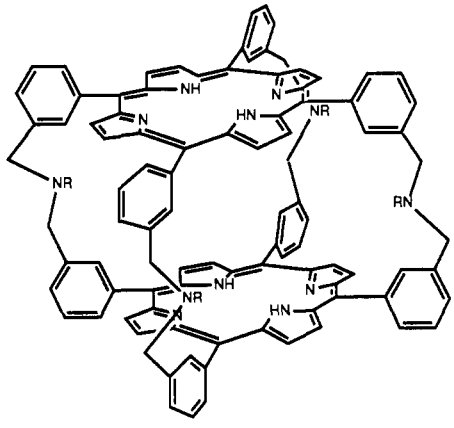

1 R = 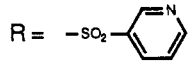 , **2** R = 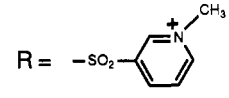

3 R = C(O)NH$_2$, **4** R = CN

5 R = 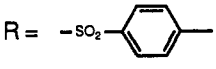

initiated with "screwed-down" geometries (Figure 1), and extensive minimization was followed by CHARM$_m$ molecular dynamics. The calculated global minima structures were analyzed in terms of the center-to-center distances (Ct–Ct), interplanar distances (P–P), and lateral shifts (LS) (see Figure 2 and Table I). Inspection of the optimum minimized dimer structures of **1**–**5** indicates that they have approximate D_4 symmetry, resulting from a screwing down action of one porphyrin core to approach the other (Figure 1). The dihedral angle $\theta_{N1Ct1Ct2N2}$ (see c of Figure 1) observed as a result of the screwed-down conformation is 26°. This angle coincides with the calculated optimal angle of closest cofacial proximity for two covalently unlinked tetraphenylporphyrin cores.[4] Incidentally, the $\theta_{N1Ct1Ct2N2}$ angle reflects the extent to which the linker can be stretched or folded in the dimers. As the interplanar distance becomes smaller, due to the approach of the porphyrin rings, the total energy decreases until an energy minimum is

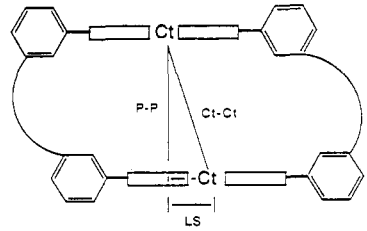

Figure 2. Schematic representation of the geometrical parameters used to describe the cofacial TPP dimers. Ct–Ct, center-to-center distance. P–P, interplanar separation. LS, lateral shift.

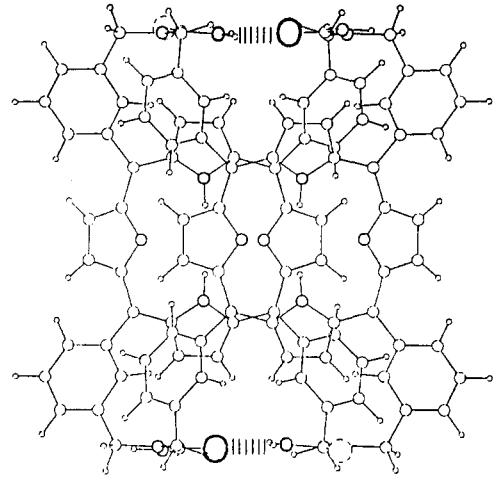

Figure 3. Top view of the CHARM$_m$-calculated global minimum structure for dimer **3**. Considerable slipping of the porphyrin planes occurs as a result of intramolecular hydrogen bonds (dotted lines) between adjacent urea side chains.

Chart II. Diurea-Linked Binary Biscobalt Porphyrin

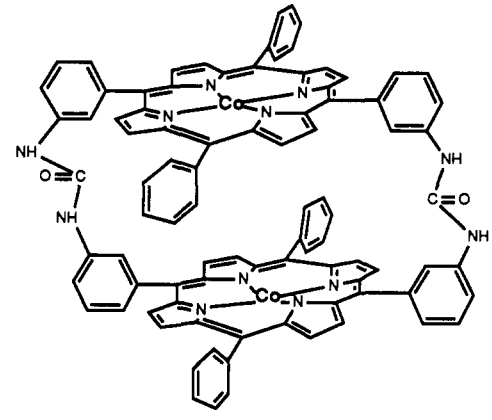

(3) Brooks, B. R.; Bruccoleri, R. E.; Olafson, B. D.; States, D. J.; Swaminathan, S.; Karplus, M. *J. Comput. Chem.* **1983**, *4*, 187.
(4) Karaman, R.; Almarsson, Ö.; Bruice, T. C. *J. Org. Chem.* **1992**, *57*, 1555.

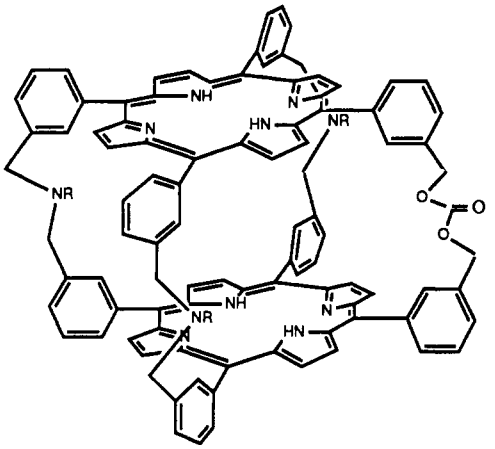

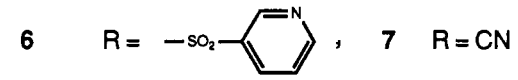

reached. A closer approach of the porphyrin planes leads to van der Waals repulsion. Further, the dynamics calculation results reveal that the peripheral substituent (i.e., for structures **1–7** the substituent R) on the linker determines the size and the shape of the cavity between the two porphyrin cores. Both the steric and electronic effects of R play dominant roles in determining the global minimum structure. The larger R, the smaller the Ct–Ct distance. Thus, with **1** and **5**, the Ct–Ct distance is shorter than with **4** (see Table I). Moreover, the more sp^3 character the bridging nitrogen displays, the more flexible the geometry, and hence, the Ct–Ct distance is shorter. The calculations show symmetrical dimers **1–5** to have D_4 symmetry with a small lateral shift. An exception is dimer **3** in which the global minimum structure exhibits a large lateral shift (Figure 2). This large lateral shift is brought about by two hydrogen bridges between adjacent amide side chains (Figure 3). Porphyrin **4** was found to be quite extended due to the bridging nitrogens being almost complete sp^2 centers. The arylsulfonate side-chain substituents seem to be best suited for effecting the smallest observed Ct–Ct distance. $CHARM_m$ gas-phase calculations show *p*-toluenesulfonamide and *m*-pyridinesulfonamide (see **1** and **5**) groups act similarly because they are essentially isosteric. Their bulky nature forces the linker units into optimally folded conformations, and the interplanar and center-to-center distances approach 5.0 Å. It is expected that the steric effect of *m*-pyridinesulfonamide and the corresponding *N*-methylpyridine derivative will be about the same, resulting in a similar calculated Ct–Ct distance for the corresponding dimers (**1** and **2**); however, the calculations show a larger Ct–Ct distance for **2** presumably due to the fact that its geometry in the gas phase exhibits a larger interplanar separation than the solution structure in order to disperse the positive charges more effectively.

Although CPK models show that very little free space exists between the porphyrin planes of **1**, "breathing motion" observed in dynamics animations is expected to make possible the entry of small molecules into the cavity. Model building also establishes that the geometry for the global minimum calculated for **1** is well suited for binding a molecule of dioxygen to two cobalt atoms placed in the center of each porphyrin ring. The resulting complex, shown in Figure 4, has Co–O bond lengths of 1.8 Å, an O–O bond length of 1.4 Å (as in a peroxo complex[5]), and a Co–O–O bond angle of 149°. Such a complex has been invoked as an intermediate in the electroreduction reactions that cofacial porphyrin dimers catalyze.[2] The porphyrin cores in the unsymmetrical dimers **6** and **7** (Figure 5) were relatively slipped, being perturbed by the long and rigid carbonate leg. The symmetry in dimers **6** and **7** is reduced to approximate C_2 symmetry, and the Ct–Ct distances become larger as anticipated (5.52 Å for **6** and 5.36 Å for **7**).

(5) Scheidt, W. R.; Lee, Y. J. *Structure Bonding* **1987**, *64*, 1–71.

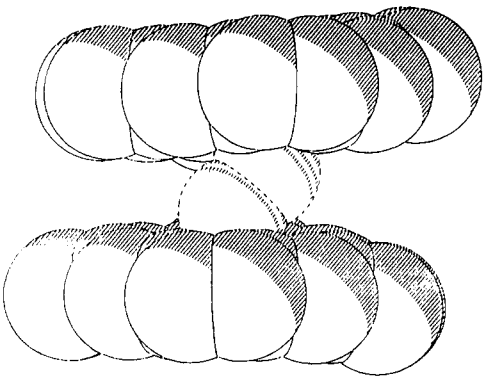

Figure 4. Hypothetical μ-peroxo bridged biscobalt porphyrin dimer **1** (protons, phenyl rings, and linkers omitted for clarity). Co–O distances are 1.8 Å; O–O distance is 1.4 Å. Co–O–O angle is 149°.

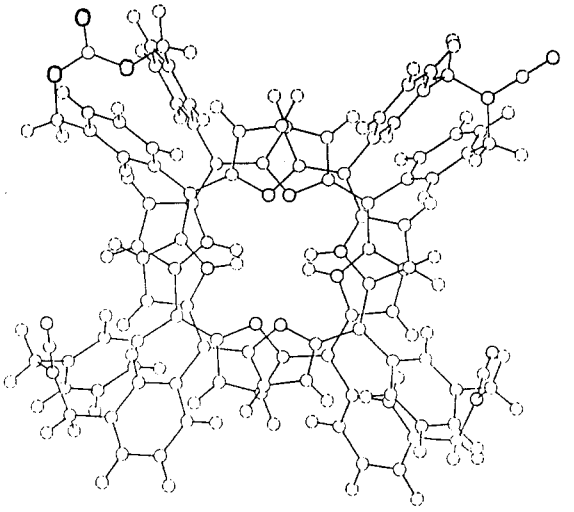

Figure 5. Top view of the $CHARM_m$-calculated global minimum structure for dimer **7**.

Electroreduction of Dioxygen Catalyzed by Cofacial Biscobalt Tetraphenylporphyrin Dimers Studied at the Rotating Ring–Disk Electrode (RRDE). The cobalt dimeric porphyrins Co_2-**1** to Co_2-**4** and Co_2-**6** were carefully evaporated onto the graphite disk electrode surface from DMF or CH_2Cl_2 solutions. After coating, the electrode was immersed into a dioxygen-saturated aqueous solution of 0.1 N H_2SO_4, and cyclic voltammograms were recorded to determine the potentials for the dioxygen reduction at the disk electrodes. Unfortunately, an estimation of formal potentials of the biscobalt porphyrins by this means was not feasible because voltammetric responses from the electrodes adsorbed with the cobalt porphyrins in the absence of dioxygen were not measurable. Our studies with adsorbed catalysts were, therefore, restricted to the voltammetric responses they produce in the catalytic reduction of dioxygen.

The catalytic peak potentials for the reduction of dioxygen at the disk electrode are summarized in Table II (see column 2). The dependence of peak potentials for dioxygen reduction on the nature of the cofacial biscobalt porphyrins is very slight. Further, the potentials were found to be comparable for monomeric cobalt porphyrin (Co-**8**) and cofacial biscobalt porphyrins. Electrochemical reduction of O_2 can occur at the disk electrode by a $2e^-$ process to yield H_2O_2 as an intermediate or via a $4e^-$ reduction to provide H_2O. In all experiments, the potential of the ring electrode was held at +1.1 V in order to detect the formation of H_2O_2. The fraction of dioxygen reduced to hydrogen peroxide was determined by the ratio of ring-to-disk currents and ring collection efficiency. RRDE voltammograms obtained from electrodes adsorbed with cobalt porphyrins Co-**8**, Co_2-**6**, and Co_2-**2** are shown in Figure 6, and the derived electrochemical data are summarized in Table II. In the absence of cobalt porphyrins, no electrode reduction of dioxygen was observed within the range

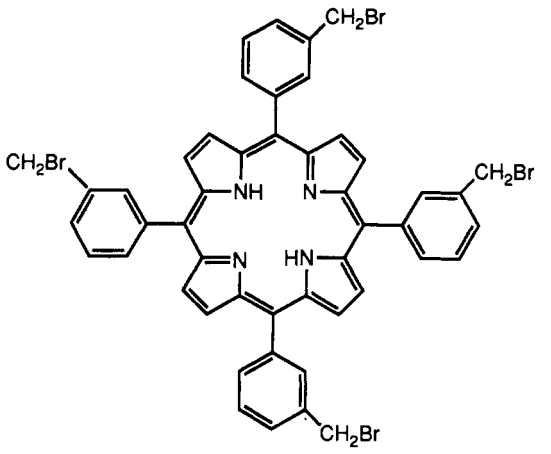

8

of potentials shown in Figure 6.

Electrochemical results with porphyrin electrodes in aqueous solutions containing 1 mM hydrogen peroxide in the absence of dioxygen establish that biscobalt porphyrin dimer **2** catalyzes the electroreduction or disproportionation of hydrogen peroxide. The intercept value of the Koutecky–Levich plot at the electrode adsorbed with Co_2-**2** as a catalyst is larger than that for dioxygen reduction. This indicates that the reduction rate of H_2O_2 is smaller than that of dioxygen and excludes unbound hydrogen peroxide as an intermediate in the reduction of dioxygen to water.

Koutecky–Levich plots of I_{lim}^{-1} (I_{lim}, limiting current density) vs $\omega^{-1/2}$ (ω, the rotation rate) for dioxygen reduction measured at rotating graphite disk electrodes adsorbed with the cobalt porphyrins are shown in Figure 7 along with the calculated lines for $2e^-$ and $4e^-$ reductions. An excellent linearity is observed between I_{lim}^{-1} and $\omega^{-1/2}$. Values of I_{lim} for the catalyzed reduction are expressed by the Koutecky–Levich equation[7] (eqs 1 and 2),

$$1/I_{lim} = 1/I_{lev} + 1/I_{kin} \quad (1)$$

$$I_{lev} = 0.2nFD^{2/3}v^{-1/6}C_o\omega^{1/2} \quad (2)$$

where I_{lev} is the limiting current density when the reaction is totally mass transfer controlled and I_{kin} is the kinetic current. The number of electrons transferred, n, is calculated from the slope of the Koutecky–Levich plot using the following values: v is the kinematic viscosity of the electrolyte solution, 0.01 cm/s; D is the diffusion coefficient of dioxygen, 1.7×10^{-5} cm^2/s; C_o is the concentration of dioxygen, 1.2 mM. The n values calculated from the slopes of Koutecky–Levich plots are slightly different from those obtained from the ratio of ring-to-disk limiting currents (see column 5 in Table II). This discrepancy seems to arise from the samll collection efficiency during the oxidation of hydrogen peroxide at the ring electrode.[1c] The rate of the chemical reaction of the reduced cobalt porphyrins and O_2 was determined from the intercept of Koutecky–Levich plots by eq 3, where k is the

$$I_{kin} = nk\Gamma_{dimer}FC_o \quad (3)$$

rate constant for the catalyzed reduction and Γ_{dimer} is the concentration of cofacial biscobalt porphyrin dimer on the electrode surface. The surface concentration of a catalyst (2×10^{-10} mol cm^{-2}) on the disk electrode is estimated from the amount of cobalt porphyrin in a small volume of stock solution and the electrode surface area. Using the method of Collman and co-workers,[1h] who showed that the reduction of dioxygen is first order in catalyst and dioxygen, the second-order rate constant for electroreduction of dioxygen in the presence of the biscobalt porphyrin dimers was calculated to be $(2 \pm 1) \times 10^5$ M^{-1} s^{-1}. This value differs slightly along the series of the biscobalt porphyrin catalysts employed.

Examination of Table II reveals that all the biscobalt porphyrin dimers studied catalyze the reduction of dioxygen at the graphite disk electrode. The magnitude of the disk limiting current and the fraction of dioxygens which undergo $2e^-$ and $4e^-$ reduction

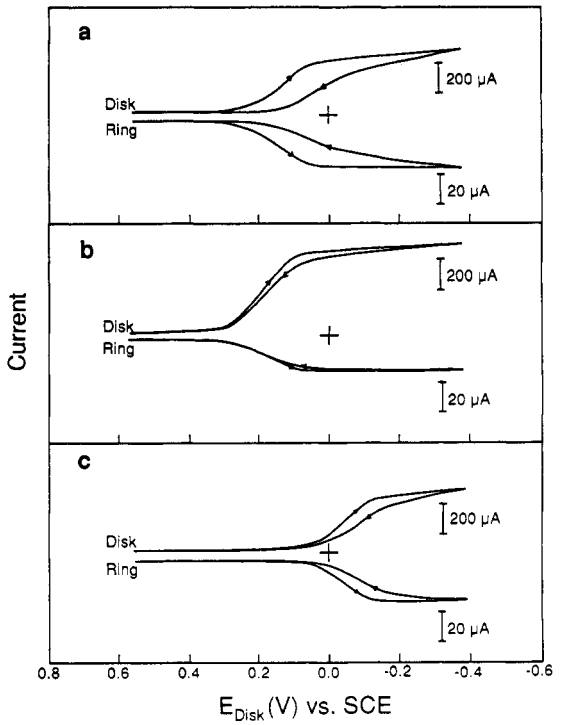

Figure 6. Ring–disk current–potential curves for dioxygen reduction at electrodes adsorbed with cobalt porphyrins in 0.1 N H_2SO_4 aqueous solutions saturated with O_2 at 1 atm. Scan rate (v) 20 mV/s. Ring potential 1.1 V vs SCE. Rotation rate (w) 100 rpm. (a) Monomeric cobalt porphyrin **8**; (b) dimeric cobalt porphyrin **2**; (c) dimeric cobalt porphyrin **6**.

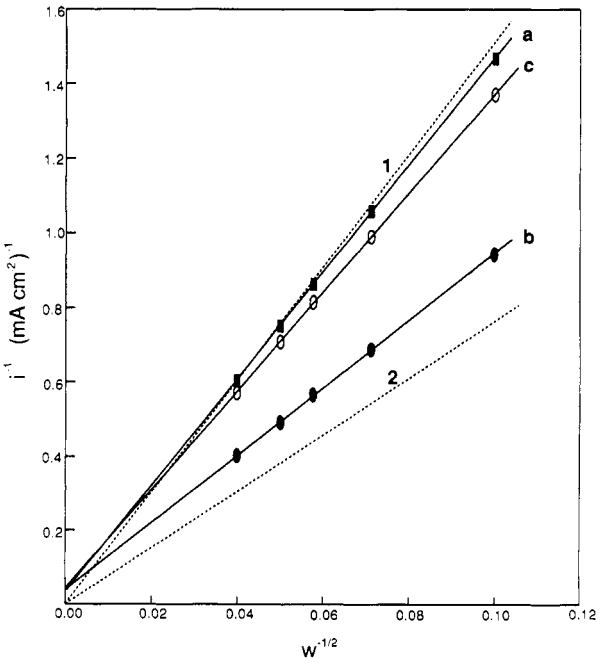

Figure 7. Koutecky–Levich plots for O_2 reduction catalyzed by cobalt porphyrins in 0.1 N H_2SO_4 aqueous solutions saturated with O_2 at 1 atm. The dashed lines (1 and 2) were calculated for the diffusion–convection limited reduction by two and four electrons, respectively. (a) Monomeric cobalt porphyrin **8**; (b) dimeric cobalt porphyrin **2**; (c) dimeric cobalt porphyrin **6**.

depend on the nature of the biscobalt porphyrin dimer. As expected, O_2 reduction catalyzed by the monomeric porphyrin Co-**8** mainly occurs through the $2e^-$ reduction pathway, resulting in the formation of hydrogen peroxide. The unsymmetrical biscobalt porphyrin dimer **6** shows monomer-like catalytic activity. The similarity between **6** and the monomeric porphyrin is attributed

Table I. ^{1}H NMR and UV/Visible Spectral Data and CHARM$_m$-Calculated Properties[a] of Quadruply Linked Dimers

compd	Ct–Ct[e]	P–P[e]	LS[e]	^{1}H NMR δ N–H[b]	^{1}H NMR δ′ N–H[c]	^{1}H NMR δ H-2′[b]	UV/vis W[d]
1	5.03	5.00	0.28	−4.34	−5.4[g]	7.04	18.9
2[f]	5.60	5.54	0.27		−5.8[g]		
3	5.15	4.39	2.69		−4.35	6.95[c]	20.0
4	5.75	5.73	0.20	−3.98	−4.0	7.31	18.1
5	5.03	4.99	0.67	−4.42		7.14	19.1
6[f]	5.52	5.32	1.46	−3.95	−3.95		19.0
7[f]	5.36	5.35	0.34	−3.80			17.0
8				−2.81		8.21	12.0

[a] All distances are in Å. [b] Chemical shifts in ppm relative to TMS. Solvent used is $CDCl_3$ unless otherwise indicated. [c] Solvent used is DMSO-d_6. [d] Soret bandwidth at half-height in nm. [e] Ct–Ct is the center-to-center distance, P–P is the interplanar distance, and LS is the lateral shift (see Figure 2). [f] These have more than one H-2′ resonance. [g] Chemical shift was determined at 150 °C in DMSO-d_6.

Table II. Dioxygen Electrocatalytic Properties at Electrodes Adsorbed with Cobalt Tetraphenylporphyrins

porphyrin	$E_{p,cat}$[a]	% H_2O_2 (n)[b]	I_{lim}[c]	n[d]
Co_2-**1**	+0.10	34.0 ± 3.0 (3.3)	0.94	3.1 ± 0.2
Co_2-**2**	+0.11	30.1 ± 3.0 (3.4)	1.06	3.3 ± 0.2
Co_2-**3**	+0.04	51.8 ± 3.0 (3.0)	0.76	2.5 ± 0.2
Co_2-**4**	+0.08	51.1 ± 3.0 (3.0)	0.78	2.6 ± 0.2
Co_2-**6**	−0.12	68.7 ± 5.0 (2.6)	0.72	2.3 ± 0.2
Co-**8**	+0.07	69.8 ± 5.0 (2.6)	0.69	2.1 ± 0.2

[a] Dioxygen electrocatalytic peak potential ($E_{p,cat}$ vs SCE) at graphite disk electrode at scan rate 0.1 V s^{-1}. [b] Calculated from % $H_2O_2 = (-i_r/Ni_d)100$ where i_r and i_d are the ring and disk limiting currents, respectively, and N is the collection coefficient. The number of electrons transferred (n in parentheses) is calculated from $n = 4 - 2(i_r/Ni_d)$. [c] Limiting current density (mA cm^{-2}) for the reduction of dioxygen at 100 rpm in O_2-saturated solutions. [d] Evaluated from the slopes of Koutecky–Levich plots for dioxygen reductions with the catalysts.

to the long Ct–Ct distance in Co_2-**6** (above 5.3 Å) precluding any effective coordination of O_2 to effect the 4e$^-$ reduction of O_2 to water. It should be noted that the inability of biscobalt porphyrins with extended Ct–Ct distances to carry out 4e$^-$ reduction of O_2 has previously been observed.[1] For example, Collman and associates showed that porphyrin dimers A and B with long Ct–Ct

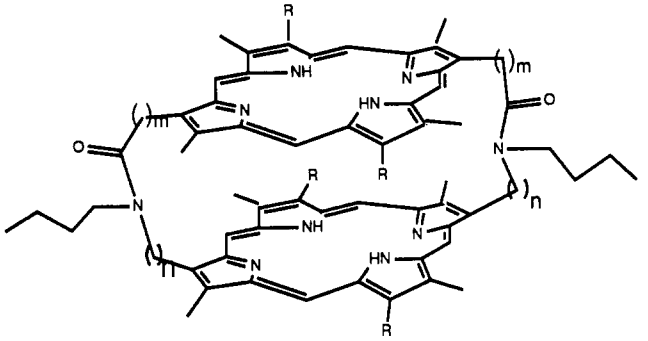

A n = 3, m = 2, R = hexyl
B n = 3, m = 1, R = hexyl
C n = 2, m = 1, R = hexyl

distances (6.4 and 5.4 Å, respectively) are not effective in reducing oxygen to water, whereas the porphyrin dimer C with a Ct–Ct distance of 4.2 Å is very effective.[1g]

Of the porphyrins examined in this study, the water-soluble symmetrical cofacial biscobalt porphyrin Co_2-**2** and its precursor, porphyrin Co_2-**1**, show the greatest 4e$^-$ reduction activity as shown in the increased disk limiting currents and the decreased detection of hydrogen peroxide (less than 34%). The Ct–Ct distances of Co_2-**1** and Co_2-**2** are the shortest (less than 5 Å)[6] of the dimeric

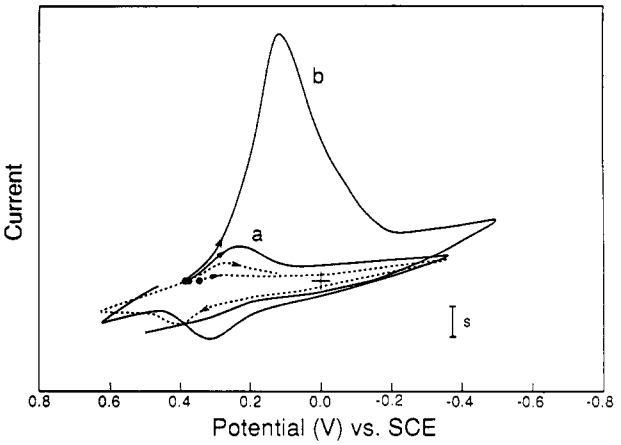

Figure 8. Cyclic voltammograms at the pyrolytic graphite disk electrode in dissolved cofacial cobalt porphyrin **2**. (a) Solution saturated with argon, s = 20 μA; (b) solution saturated with dioxygen, s = 100 μA. Scan rate 0.1 V/s; supporting electrolyte 0.1 N H_2SO_4. The dashed line is the background response of the pyrolytic graphite when porphyrin is absent.

porphyrins studied.

Electrochemical studies of the reduction of O_2 by the water-soluble Co_2-2 dissolved in acidic aqueous solution, measured under argon at a highly polished pyrolytic graphite electrode, are shown in Figure 8a. As in the case of the RRDE experiments with porphyrin dimers, the solutions were 0.1 N in H_2SO_4 and contained 0.5 mM Co_2-**2**. The redox couple for Co_2-**2** in the absence of O_2 has broadened waves, implying that the two cobalt(III) centers are reduced in a stepwise manner at very close potentials. A half-wave potential ($E_{1/2}$) value of +0.29 V vs SCE was obtained by averaging the cathodic and anodic peak potentials. Repetitive scanning produces identical voltammograms, indicating that the oxidation states of the cobalt can be reversibly changed between Co(III) and Co(II). The cathodic peak current ($i_{p,c}$) is equal in magnitude to the anodic peak current ($i_{p,a}$) in thoroughly deoxygenated solutions of cofacial cobalt porphyrin **2**. Upon the addition of a small amount of dioxygen, $i_{p,c}$ is increased while $i_{p,a}$ is decreased.

To investigate the effect of Co_2-**2** on the reduction of dioxygen, cyclic voltammetry was performed in dioxygen-containing solutions of Co_2-**2**. The cyclic voltammogram obtained for Co_2-**2** in the absence of dioxygen is comparable to that obtained in the presence of dioxygen (see Figure 8). The foot of wave a in Figure 8 is close to the potential where the catalytic reduction of dioxygen (wave b) begins in oxygen-saturated solutions of Co_2-**2**. The catalytic peak potential for the reduction of dioxygen is +0.11 V, which is the same as the value obtained with a electrode doped with Co_2-**2**. The potentials for electrochemical reduction of O_2 remain

(6) The CHARM$_m$-calculated interplanar distance for dimer **7** is 5.54 Å. This overestimated value is due to the failure of CHARM$_m$ in handling cationic structures. Therefore, the interplanar distance or the center-to-center distance was estimated from eqs 5 and 7 and was found to be 4.75 Å.

(7) (a) Koutecky, J.; Levich, V. G. *Zh. Fiz. Khim.* **1958**, *32*, 1565. (b) Andrieux, C. P.; Dumas-Bouchiat, J. M.; Savieant, J. M. *J. Electroanal. Chem.* **1982**, *131*, 1. (c) Bard, A. J.; Faulkner, L. R. *Electrochemical Methods, Fundamentals and Applications*; Wiley: New York, 1980; Chapter 6.

the same regardless as to whether catalyst Co_2-**2** is free in solution or fixed at the disk of a RRDE. The fraction of dioxygen reduced to hydrogen peroxide is 29 ± 3% detected at the ring. Repetitive scanning results in a very small decrease of disk limiting current (5% decrease in 10 repetitive scans). The number of electrons transferred, $n = 3.2 \pm 0.1$, obtained from the slope of the Koutecky–Levich plot indicates 60 ± 5% electroreduction of dioxygen to water, even after prolonged exposure.

Correlations between the Interplanar Distance and Physical and Electrochemical Properties of the Free Base Forms of the Porphyrin Dimers. Considering the UV/vis spectra of bisporphyrins, it has been shown that the magnitude of exciton coupling, as it is reflected by the broadining of the Soret absorption, is determined by the closeness of the two porphyrin cores[4,8] (see Table I). This is supported by the linear relationship which we find between the width of the Soret absorption (W) and the gas-phase calculated interplanar distances (P–P) (see Table I and eq 4). As it is shown

$$\text{P–P} = -0.70W + 18.45 \qquad R = 0.94 \qquad (4)$$

in eq 4, the values of the Soret band width are large when the two porphyrin cores in the dimer are in close proximity (short interplanar distance). Thus, from eq 4 the increase in the bandwidth of the Soret absorption serves as a good index for the estimation of the closeness of the two porphyrin cores. The ^{1}H NMR spectra of the porphyrin dimers **1–7** display resonances that are significantly upfield shifted when compared to those of the corresponding monomeric porphyrin **8** (Table I). The upfield shift in the chemical shifts of the pyrrolic N–H resonances is about 2.5 ppm and that of ortho phenylic H (H-2′) resonances is about 1.3 ppm (see Table I). As anticipated, the gradual upfield shift of the pyrrolic N–H resonances and ortho phenylic H in the series of the dimers studied (Table I) results from a decrease in separation between the two porphyrin rings; one porphyrin core experiences more of the shielding effect of the other as it comes closer to its shielding region.[7] Further, the CHARM$_m$-calculated interplanar distances (P–P) of porphyrin dimers **1–7** (see Table I) have been shown to correlate reasonably well with the ^{1}H NMR chemical shifts of the pyrrolic N–H (δ N–H) and the ortho phenylic H resonances (δ H-2′) eqs 5 and 6 respectively.[4]

$$\text{P–P} = 0.88(\delta\ \text{N–H}) + 8.85 \qquad R = 0.96 \qquad (5)$$

$$\text{P–P} = 3.41(\delta\ \text{H-2}') - 19.20 \qquad R = 0.96 \qquad (6)$$

Comparison of the slopes of eqs 5 and 6 indicates that the H-2′ resonances experience more of the shielding effect of the magnetic anisotropy of the two porphyrin rings than that of the pyrrolic N–H. This is in good agreement with CHARM$_m$-calculated global minima structures of **1–5** which show the ortho phenylic protons (H-2′) to be more directed into the shielding cone of the porphyrin cores than the pyrrolic N–H protons, and the average distance between the H-2′ protons and the plane of the opposite porphyrin ring is considerably shorter (4 Å) than the interplanar distances (around 5 Å).

A linear correlation exists between ^{1}H NMR chemical shifts of the N–H resonances (δ' N–H) of DMSO-d_6 solutions of the dimers (Table I) and the number of electrons (Table II) transferred (n) in the reduction of dioxygen catalyzed by their corresponding biscobalt porphyrin derivatives (eq 7 and Figure 9).

$$\delta'\ \text{N–H} = -1.94n + 0.67 \qquad R = 0.96 \qquad (7)$$

As previously mentioned, the N–H resonances (δ' N–H) correlate reasonably well with the calculated gas-phase interplanar distance (see eq 5). Thus, the percentage of the 4e$^-$ reduction of O_2 is high for the dimers having interplanar distances of 5 Å such as **1** and **2**, whereas for those having long interplanar distances (above 5.3 Å) such as **4** the percentage of the 2e$^-$ reduction is dominant.

(8) (a) Karaman, R.; Bruice, T. C. *J. Org. Chem.* **1991**, *56*, 3470. (b) Bookser, B. C.; Bruice, T. C. *J. Am. Chem. Soc.* **1991**, *113*, 4208. (c) Chang, C. K. *J. Heterocycl. Chem.* **1977**, *14*, 1285. (d) Collman, J. P.; Elliott, C. M.; Halbert, T. R.; Tovong, B. S. *Proc. Natl. Acad. Sci. U.S.A.* **1977**, *74*, 18.

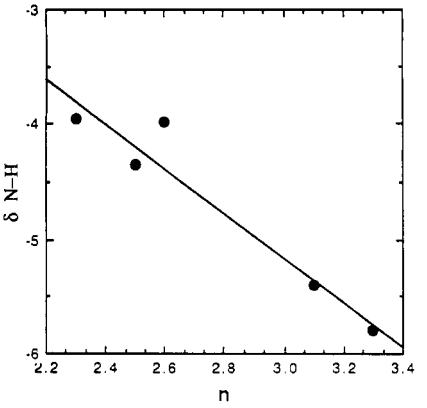

Figure 9. Plot of the ^{1}H NMR chemical shifts of the N–H resonances of the porphyrin dimers in DMSO-d_6 δ' N–H vs the number of electrons transferred (n) in the reduction of dioxygen catalyzed by their biscobalt derivatives.

Summary and Conclusions

Linear relationships are observed between the ^{1}H NMR chemical shifts of pyrrolic N–H and both the gas-phase calculated interplanar distances and the number of electrons transferred (n) in the reduction of dioxygen catalyzed by biscobalt porphyrin dimers. The electrochemical results show that biscobalt porphyrin dimers Co_2-**1** to Co_2-**4** and Co_2-**6** bind dioxygen and consequently reduce it via two different paths: through 4e$^-$ reduction to form water and via 2e$^-$ reduction to give hydrogen peroxide. The linear relationship observed between the solution ^{1}H NMR chemical shift of N–H and the number of electrons transferred (n) in the dioxygen reduction indicates that the interplanar distance in the dimers is a crucial factor for determining the electroreduction pathway. Biscobalt porphyrin dimers with appropriate interplanar distances and high field N–H chemical shifts catalyze the reduction of dioxygen mainly through the 4e$^-$ pathway, whereas those with long interplanar distances and low field N–H chemical shifts do via the 2e$^-$ path. The finding that the reduction rate of dioxygen to water is greater than that of hydrogen peroxide excludes the intermediacy of the latter in these processes. In contrast to the observations[1] of Collman and Chang, the peak potentials for oxygen reductions for the series of biscobalt dimers are generally comparable to those of monomeric species, which are not capable of four-electron reduction to water; therefore, it is believed that the precise structure of the dimeric species is the dominant factor governing the catalytic properties of these systems. The following remarks emerge from this study: (1) The precise geometrical nature of the biscobalt tetraphenylporphyrin dimers, and not their catalytic peak potentials, appears to be the crucial factor determining their activity in the 4e$^-$ reduction of oxygen to water. (2) The dimeric porphyrins presented herein represent the first effective rigid water- and non-water-soluble porphyrin dimer system to catalyze 4e$^-$ reduction of dioxygen to water.

Experimental Section

General. Absorption spectra were recorded on a Cary-14 spectrophotometer interfaced to a Zenith computer equipped with OLIS (On-Line Instrument System Inc.) data acquisition and processing software. Fast atom bombardment (FAB) mass spectroscopy was performed at UCSB using *m*-nitrobenzyl alcohol as the matrix and a parallel run of cesium rubidium iodide as the reference. All reactions were carried out with purified reagents in dry, purified solvents. Column chromatography was performed with Fischer Type 60-Å (200–425-mesh) silica gel. Preparative thin-layer chromatography (TLC) was performed using E.M. Sciences Kieselgel 60 F_{254}.

Electrochemistry. Cyclic voltammetric measurements were performed with a three-electrode potentiostat (Bioanalytical Systems, Model CV-27) and were recorded on Houston Instruments Model 100 Omnigraphic. A platinum wire electrode separated from the analyte compartment by a medium porosity glass frit was used as the auxiliary electrode. A Ag/AgCl electrode, filled with aqueous tetramethylammonium chloride solution and standaridized to 0.00 V vs SCE with a solution junction via a Pyrex glass tube closed with a soft glass cracked bead contained in a luggin capillary, was used as the reference electrode. A pyrolytic graphite

(0.46-cm²) disk electrode was employed as the working electrode. Rotating ring-disk experiments were conducted using a RDE4 instrument (Pine Instrument Company). A pyrolytic graphite disk/platinum ring electrode was used. The ring collection efficiency ($N = 0.17$) was determined using a solution of ferrocene. All working electrode surfaces were highly polished with alumina paste prior to each experiment. Adsorption of metalloporphyrins was accomplished by dropping organic solvents containing metalloporphyrins on the disk electrode, followed by careful evaporation of the solvent. Aqueous solutions of water-soluble porphyrins were prepared using distilled-deionized water with less than 0.5% *N,N*-dimethylformamide (DMF). Dioxygen concentrations in O_2-saturated solutions were assumed to be 1.2 mM at room temperature. Solutions of 0.1 N H_2SO_4 were used as supporting electrolytes. All reported potentials are with respect to a saturated calomel electrode (SCE).

Theoretical Calculations. All model building and calculations were performed on a Silicon Graphics IRIS 4D/220 GTX workstation, using the programs Quanta version 3.2 (Polygen Corp.) and CHARM$_m$[3] version 21.2. The topology file PORPHYRINH.RTF supplied by Polygen was used as a basis for the porphyrin moieties of the dimers, and the linkers were constructed in Chemnote, the 2D modeling facility in Quanta. Minimizations were performed using the steepest descent algorithm, followed by an adopted basis Newton-Raphson algorithm, until the energy change tolerance was less than 10^{-9} kcal/mol. The nonbonded interaction cutoff distance and hydrogen bonding cutoff distance were chosen to be 11.5 and 7.5 Å, respectively. Molecular dynamics were performed using Verlet integration and the SHAKE algorithm to fix C-H bonds. At 600 K, the maximum allowable fluctuation in temperature was fixed at 25 K. Nonbonded interaction and hydrogen bond lists were updated every 0.05 ps.

Preparation of Co_2-1. A mixture of **1**[9] (20 mg, 0.0102 mmol) and $CoCl_2 \cdot 6H_2O$ (100 mg, 0.42 mmol) was heated at 135 °C for 5 h and then diluted with chloroform (100 mL) and methanol (25 mL). The reaction mixture was extracted with 5% aqueous ammonium hydroxide solution, water, and brine, and the organic layer was separated, dried over anhydrous Na_2SO_4, filtered, and evaporated to give 19 mg (90.4%) of Co_2-**1** as a deep orange powder: FABMS m/z 2071 (calcd for $C_{116}H_{80}N_{16}O_8S_4Co_2$ [M^+] m/z 2070.5); UV/vis (DMF) λ_{max} ($\epsilon \times 10^{-3}$ cm^{-1} M^{-1}) 409 (121), 529 (17.7).

Preparation of Co_2-2. A mixture of **2**[9] (10 mg, 0.0049 mmol) and $CoCl_2 \cdot 6H_2O$ (50 mg, 0.21 mmol) in DMF (5 mL) was heated at 135 °C for 6 h. The reaction mixture was evaporated, and the resulting green residue was triturated with cold water, filtered, washed with ether, and dried to give 9.8 mg (93.3%) of Co_2-**2** as a deep orange powder: FABMS m/z 2115 (calcd for $C_{119}H_{89}N_{16}O_8S_4Co_2$ [$M^+ - CH_3$] m/z 2115.5); UV/vis (DMF) λ_{max} ($\epsilon \times 10^{-3}$ cm^{-1} M^{-1}) 409 (300), 530 (28.3).

Preparation of Co_2-3. A mixture of **3**[9] (10 mg, 0.0064 mmol) and $CoCl_2 \cdot 6H_2O$ (50 mg, 0.21 mmol) in DMF (20 mL) was heated at 120 °C for 48 h. The reaction mixture was evaporated to dryness, and the reddish residue was triturated with water (100 mL × 3), collected, washed with ether, and dried at 25 °C/0.2 mmHg to give 9.2 mg (85.7%) of Co_2-**3** as a reddish powder: FABMS m/z 1678 (calcd for $C_{100}H_{72}N_{16}O_4Co_2$ (M^+) m/z 1678.5); UV/vis (DMF) λ_{max} ($\epsilon \times 10^{-3}$ cm^{-1}) 409 (267), 529 (17.8).

Preparation of Co_2-4. A mixture of **4**[9] (18 mg, 0.012 mmol) and $CoCl_2 \cdot 6H_2O$ (50 mg, 0.21 mmol) in DMF (10 mL) was heated at 95 °C for 8 h and then diluted with chloroform (100 mL). The reaction mixture was extracted with water and brine, dried over anhydrous Na_2SO_4, filtered, and evaporated to yield a deep orange powder. The resulting orange residue was subjected to silica gel column eluting with a mixture of chloroform/methanol (100:3). The nonpolar orange band was collected to give 17 mg (87.6%) of Co_2-**4** as a deep orange powder: UV/vis ($CHCl_3$) λ_{max} ($\epsilon \times 10^{-3}$ cm^{-1} M^{-1}) 406 (320), 530 (27.7); FABMS m/z 1607 (calcd for $C_{100}H_{64}N_{16}Co_2$ [M^+] m/z 1606.4).

Preparation of Co_2-6. A mixture of **6**[9] (10 mg, 0.0054 mmol) and $CoCl_2 \cdot 6H_2O$ (50 mg, 0.21 mmol) in DMF (30 mL) was heated at 120 °C for 48 h and then diluted with chloroform (200 mL). The reaction mixture was extracted with water and brine, dried over anhydrous Na_2SO_4, filtered, and evaporated to yield 9.7 mg (91.5%) of Co_2-**6** as a deep orange powder: FABMS m/z 1974 (calcd for $C_{112}H_{76}N_{14}O_9S_3Co_2$ [M^+] m/z 1974.4); UV/vis (DMF) λ_{max} ($\epsilon \times 10^{-3}$ cm^{-1} M^{-1}) 410 (209), 530 (16.7).

Preparation of Co-8. A mixture of **8**[8b] (50 mg, 0.051 mmol), $CoCl_2 \cdot 6H_2O$ (100 mg, 0.42 mmol), and NaBr (1 g) in DMF (20 mL) was heated at 80 °C for 24 h and then diluted with chloroform (200 mL). The reaction mixture was extracted with water and brine, and the organic layer was separated, dried over anhydrous Na_2SO_4, filtered, and evaporated to yield an orange powder. The resulting orange residue was subjected to silica column eluting with a mixture of chloroform/methanol (100:3). The nonpolar band was collected to give 28 mg (53%) of Co-**8** as deep orange powder: UV/vis ($CHCl_3$) λ_{max} ($\epsilon \times 10^{-3}$ cm^{-1} M^{-1}) 410 (151), 528 (20.5); FABMS m/z 1039 (calcd for $C_{48}H_{32}Br_4N_4Co$ [M^+] m/z 1038.9).

Acknowledgment. This study was supported by grants from the National Institute of Health and Protos Corporation of Emeryville, CA.

Registry No. 1, 134260-60-9; Co_2-**1**, 141090-89-3; **2**, 134209-10-2; Co_2-**2**, 141090-90-6; **3**, 138312-89-7; Co_2-**3**, 141090-91-7; **4**, 133672-00-1; Co_2-**4**, 141090-92-8; **5**, 133671-99-5; **6**, 138312-91-1; Co_2-**6**, 141090-93-9; **7**, 138312-92-2; **8**, 133671-91-7; Co-**8**, 141090-94-0; O_2, 7782-44-7.

(9) Karaman, R.; Blaskó, A.; Almarsson, Ö.; Arasasingham, R.; Bruice, T. C. *J. Am. Chem. Soc.*, preceding paper in this issue.

Communications to the Editor

An Alternate Geometry for the Catalytic Triad of Serine Proteases

David R. Corey,† Mary E. McGrath,‡ John R. Vásquez,† Robert J. Fletterick,*,‡ and Charles S. Craik*,†,‡

Department of Pharmaceutical Chemistry and Department of Biochemistry, University of California San Francisco, California 94143-0446

Received January 31, 1992

The catalytic triad of serine proteases, Asp-His-Ser, is one of the classic motifs of enzymology. Effective strategies for the incorporation of the triad into non-protease protein scaffolds (i.e., antibodies[1] or de novo designed peptides[2]) might allow the development of sequence-specific peptidases or other novel enzymes. Such catalyst design would be facilitated by knowledge of the limits within which the orientation or composition of the triad members can be altered while still preserving significant peptidase activity.

We have previously reported that, of the three members of the triad, only the serine in trypsin is necessary for a minimal level of catalysis toward peptide bonds.[3] In this communication we report the mutation of Asp 102 and the partial replacement of its function in catalysis through the introduction of aspartic or glutamic acid in place of a neighboring amino acid, Ser 214. The

* Authors to whom communication should be addressed.
† Department of Pharmaceutical Chemistry.
‡ Department of Biochemistry.

(1) (a) Lerner, R. A.; Benkovic, S. J.; Schultz, P. G. *Science* **1991**, *252*, 659-667. (b) Lewis, C. T.; Hilvert, D. *Curr. Opin. Struct. Biol.* **1991**, *1*, 624-629.

(2) (a) DeGrado, W. F.; Wasserman, Z. R.; Lear, J. D. *Science* **1989**, *243*, 622-628. (b) Hahn, K. W.; Klis, W. A.; Stewart, J. M. *Science* **1990**, *248*, 1544-1547. (c) Sander, C. *Curr. Opin. Struct. Biol.* **1991**, *1*, 630-637. (d) DeGrado, W. F.; Raleigh, D. P.; Handel, T. *Curr. Opin. Struct. Biol.* **1991**, *1*, 984-993.

(3) Corey, D. R.; Craik, C. S. *J. Am. Chem. Soc.* **1992**, *114*, 1784-1790.

0002-7863/92/1514-4905$03.00/0